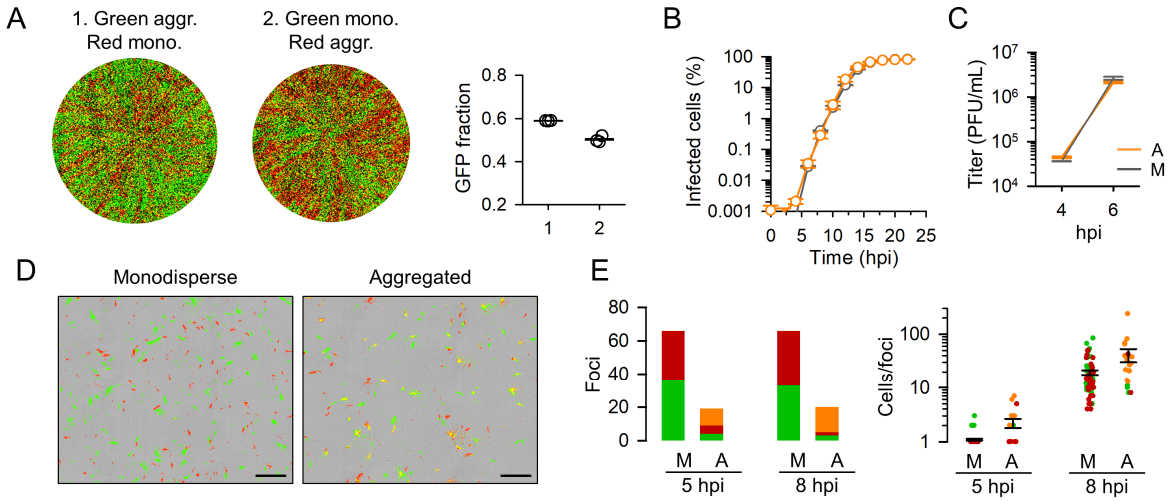

Figure S1. Fitness effect of viral aggregation in BHK-21 cells, Related to Figure 1.
A. Whole-well fluorescence microscopy images of cultures inoculated with aggregated VSV-GFP and monodisperse VSV-mCherry particles (1), and with monodisperse VSV-GFP and aggregated VSV-mCherry particles (2). Images correspond to one of the three replicate assays performed. The fraction of the total fluorescent area occupied by GFP-positive cells is shown on the right graph for the three replicates. Error bars: SEM. Populations founded by aggregates were significantly fitter than those founded by monodisperse particles (t-test: $P < 0.001$). **B.** Growth curve of VSV in BHK-21 cells obtained by real-time whole-well fluorescence microscopy. The percentage of fluorescent cells in the well is shown. Orange: aggregated inoculum. Grey: monodisperse inoculum. No differences between curves were detected. Three replicates were performed. Error bars: SEM. **C.** Viral titers in cultures inoculated with aggregates versus the same number of monodisperse particles. For an input of 5000 PFU/mL, the 4 hpi titers were on the order of 10^4 PFU/mL and were 1.2-fold higher on average in cultures inoculated with aggregates (t-test: $P = 0.009$), whereas the 6 hpi titers reached 5×10^5 PFU/mL and were similar in both cases ($P = 0.073$). Error bars: SEM (three replicates). **D.** Foci formation in BHK-21 cells inoculated with equal numbers of monodisperse versus aggregated particles (10 hpi). VSV-GFP and VSV-mCherry were mixed prior to aggregation. Cells expressing both VSV-GFP and VSV-mCherry appear in yellow. The cell monolayer is shown in phase contrast. Scale bar: 1 mm. As in MEFs, doubly fluorescent foci were highly frequent in cells inoculated with saliva-treated viruses, but not in cells inoculated with untreated viruses. **E.** Analysis of individual infection foci at different time points in BHK-21 cells inoculated with monodisperse (M) versus aggregated (A) particles. Left: bars indicate the number of foci positive for GFP (green), mCherry (red), or both (orange). Right: number of cells within infection foci (same color legend). As opposed to MEFs, aggregation reduced the number of infection foci. At 5 hpi, aggregates produced 19 infection foci of 2.2 ± 0.4 cells on average, whereas an equal input of monodisperse particles produced 66 foci of smaller size (1.1 ± 0.4 cells; t-test of log-transformed sizes; $P < 0.001$). Hence, aggregation had a negative impact on dispersal capacity (3.5-fold drop in the number of foci), yet produced larger infection foci. Error bars: SEM.

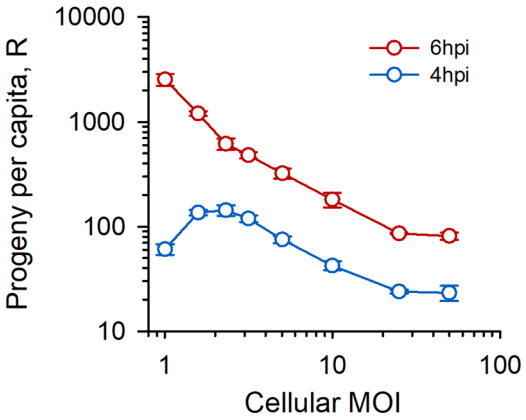

Figure S2. Effects of cellular MOI on early viral progeny production in BHK-21 fibroblasts, Related to Figure 2.

Per capita proliferation (*R*, defined as final/initial titer) for different cellular MOI values (defined as the average number of initial particles per infected cell). Viral titers were determined at 4 and 6 hpi by the plaque assay. At 4 hpi, invading cells with multiple particles was beneficial compared to single-particle infections for up to cMOI = 5 PFU/cell, and *R* peaked for cMOI of 2-3 PFU/cell. At 6 hpi, in contrast, *R* decreased monotonically with the cMOI, indicating that, at this later stage of infection, viral density was beyond the early time points in which Allee effects were detectable. Each data point is the average of three replicates. Error bars: SEM.

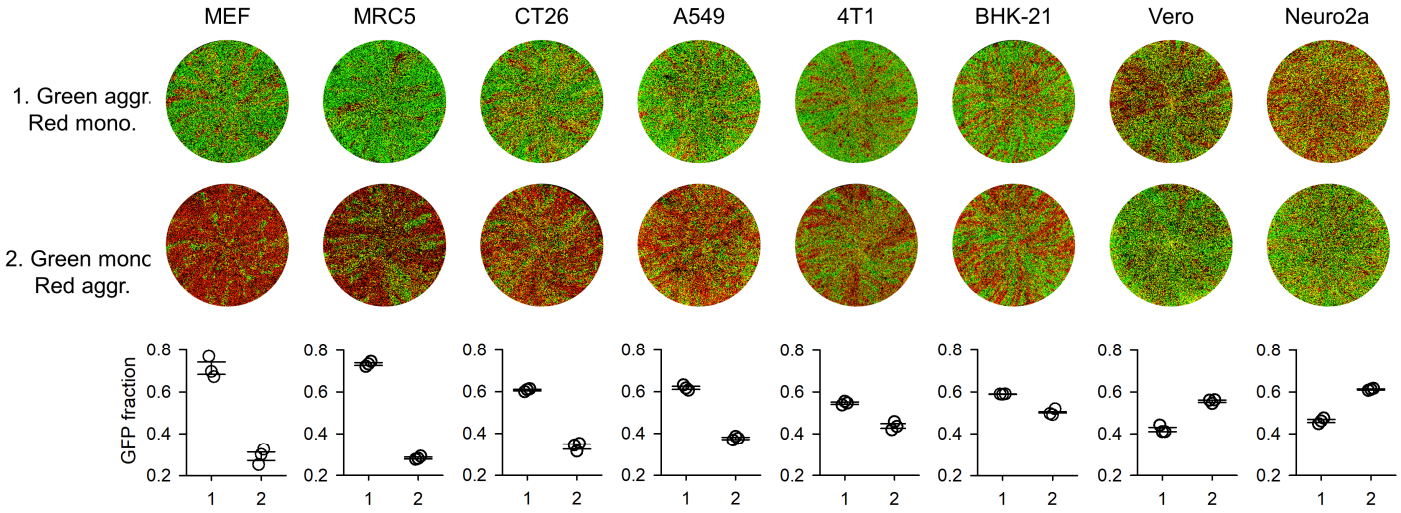

Figure S3. Fitness effect of viral aggregation in different cell types, Related to Figure 4.
Whole-well fluorescence microscopy images of cultures inoculated with aggregated VSV-GFP and monodisperse VSV-mCherry particles (1), and with monodisperse VSV-GFP and aggregated VSV-mCherry particles (2). Images were taken at the time point yielding maximal total fluorescence and correspond to one of the three replicate assays performed. The fraction of total fluorescent area occupied by GFP-positive cells is shown in the lower graphs for the three replicates. Error bars: SEM. Differences in the GFP fraction were statistically significant in all cell types (t-tests: $P < 0.001$) and revealed that aggregation was selectively advantageous in MEFs, MRC5, CT26, A549, 4T1, and BHK-21 cells, whereas it was disadvantageous in Vero and Neuro2a cells. Fitness values obtained in these assays are provided in **Table S1**.

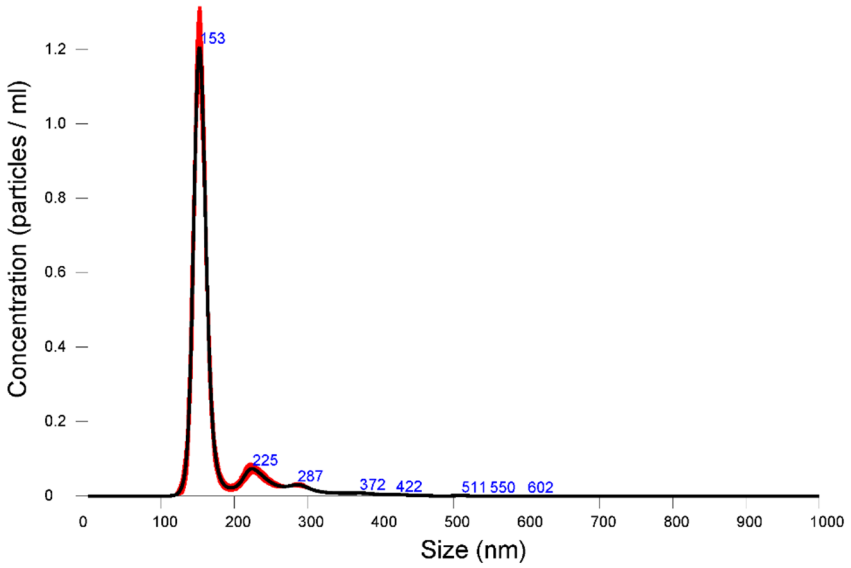

Figure S4. Nanoparticle tracking analysis of VSV virions, Related to Figure 4.
Size spectrum of gradient-purified VSV. The size distribution corresponds to the hydrodynamic diameter of the particle, and was obtained by measuring Brownian motion in five replicate videos. This provided the particle diffusion coefficient, which allows estimation of the hydrodynamic diameter using Stokes-Einstein equation. The dominant peak is consistent with the size of single viral particles, showing that, in the absence of saliva, the purified particles showed little or no aggregation at room temperature. Particle counting from videos yielded 79.8 particles/frame, which corresponded to an estimated concentration of 3.14×10^{12} particles/mL. The titer of this stock was 3.0×10^{11} PFU/mL as determined by plaque assays in BHK-21 cells. Because in these cells each foci yields a plaque, the foci formation efficiency of the virus in BHK-21 cells was 0.096 foci/particle. The foci formation efficiency in different cell types is provided in **Table S1**.

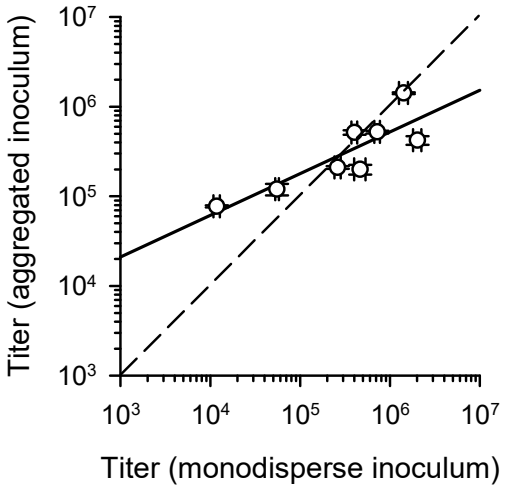

Figure S5. The fitness advantage of viral aggregation correlates with cell permissivity to infection, Related to Figure 4.

Viral titers at 6 hpi are shown for cells inoculated with monodisperse versus aggregated particles. Each dot corresponds to a different cell type. The leftmost data points correspond to MEFs and MRC5. Data for each cell type are provided in **Table S1**. The dashed line indicates equal progeny production of aggregates and monodisperse particles. The solid line indicates the least-squares log-log regression. The slope of this line is 0.463 ± 0.117, which differs significantly from 1.0 (P = 0.0025), indicating that aggregation tends to be beneficial in cells in which viral growth is less efficient. Each data point is the average of three replicates. Error bars: SEM.

Table S1. The fitness benefit of viral aggregation depends on cell permissivity and innate immunity, Related to Figure 4.

Cell line	Titer 4 hpi (× 10^4)		Titer 6 hpi (× 10^4)		Competition assays (%GFP/total)		Foci formation eff.	Endpoint titer (× 10^8)	
	Mono.	Aggr.	Mono.	Aggr.	Aggr. GFP mono Cherry[a]	Aggr. Cherry mono GFP[b]	(%foci/particle)[c]	Wild-type	Δ51
MEF	Inoc[d]	2.16 ± 0.09	1.18 ± 0.09	7.75 ± 0.22	71.3 ± 3.0	29.3 ± 2.0	1.10 ± 0.15	1.52 + 0.10	0.056 + 0.010
MRC5	Inoc[d]	Inoc[d]	5.52 ± 0.26	12.0 ± 1.8	73.3 ± 0.7	28.3 ± 0.4	1.52 ± 0.10	4.97 + 0.65	0.045 + 0.011
CT26	Inoc[d]	1.52 ± 0.19	40.2 ± 2.9	51.7 ± 3.0	60.8 ± 0.4	33.7 ± 1.1	1.93 ± 0.31	1.97 + 0.38	2.83 + 0.34
A549	1.15 ± 0.08	4.17 ± 0.15	141 ± 16	141 ± 3	61.9 ± 0.7	37.7 ± 0.5	6.69 ± 0.26	5.15 + 0.21	2.57 + 0.17
4T1	Inoc[d]	Inoc[d]	46.5 ± 6.7	20.0 ± 2.5	54.6 ± 0.5	43.7 ± 1.1	2.91 ± 0.21	5.00 + 0.20	0.185 + 0.061
BHK-21	3.60 ± 0.03	4.43 ± 0.19	261 ± 20	210 ± 8	58.9 ± 0.1	50.3 ± 0.2	9.55 ± 0.51	13.0 + 1.76	18.3 + 2.4
Vero	Inoc[d]	Inoc[d]	72.0 ± 5.1	52.2 ± 1.9	42.1 ± 1.0	55.6 ± 0.6	4.21 ± 0.98	1.33 + 0.16	3.42 + 0.26
Neuro2a	2.22 ± 0.53	1.68 ± 0.27	202 ± 21	42.2 ± 4.7	46.2 ± 0.8	61.2 ± 0.3	13.0 ± 0.2	11.8 + 1.9	20.2 + 1.6

[a]Percentage of GFP to total fluorescence in competition assays between aggregated VSV-GFP and monodisperse VSV-mCherry founder particles.
[b]Percentage of GFP to total fluorescence in competition assays between aggregated VSV-mCherry and monodisperse VSV-GFP founder particles.
[c]Percentage of particles that produce foci. Particles were quantified by nanoparticle tracking analysis, and foci were visualized by fluorescence microscopy.
[d]Equal or lower than the inoculum (0.5× 10^4 PFU/mL).